Correlation between Reynolds number and stenosis morphology in eccentric and concentric artery models

Ashkan Javadzadegan[1], Yasutomo Shimizu[2], Masud Behnia[1] and Makoto Ohta[3*]

[1] School of Aerospace, Mechanical and Mechatronic Engineering, The University of Sydney, NSW, Australia
[2] Graduate School of Biomedical Engineering, Tohoku University, Tohoku, Japan
[3*] Intelligent Fluid Systems Div, Institute of Fluid Science, Tohoku University, Tohoku, Japan
ohta@biofluid.ifs.tohoku.ac.jp

ABSTRACT

Atherosclerotic plaques within coronary arteries result in coronary stenosis which compromises blood flow to the distal myocardium and result in local physiological perturbances such as recirculation and shear stress [1]. Coronary lesion severity is often graded by the amount of lumen encroachment or stenosis it causes, and most clinical decisions are made based on lesion stenosis severity [2]. However, other lesion characteristics, such as eccentricity are determinants of both shear rate and the extent of flow recirculation in in-vitro and in computational fluid dynamics (CFD) analysis of the arteries. It has been shown that 81% of the coronary lesions studied by intravascular sonography were eccentric and the eccentric lesions are more likely to be seen in patients with cardiovascular symptoms [3].

In this study, a particle image velocimetry (PIV) method was used to analyse the effect of the eccentricity on blood flow dynamics during a transient flow cycle and also to investigate how the eccentricity impact on the flow behaviour changes as the Reynolds number changes.

Two eccentric and concentric stenosis models were manufactured from silicone (R'Tech Co., Ltd, Japan). All models were a box-type with an inner diameter of 4 mm (Fig. 1). The model sizes were based on the values of the human left main artery (LMA) and left anterior descending (LAD) [4]. The resultant models had a 70% diameter stenosis based on NASCET (North American Symptomatic Endarterectomy). The models were connected to a particle image velocimetry (PIV) circuit and an Nd:YAG solid laser (BWN-532-100E, B&W TEK Inc., USA) of wavelength 532 nm and output power 100 mW was used to produce a light sheet of 1 mm thickness in the desired area of visualization. The desired thickness and width of the light sheet were achieved by aligning a micro lens with 105 mm focal length and 2.8 F ratio (Micro-Nikkor, Nikon Co. Ltd., Japan). A pulsatile flow waveform was generated using a screw pump (NBL30PU, R'Tech Co. Ltd., Japan). At different times corresponding to different Reynolds numbers ($Re = DU/\nu$, D is the diameter of the parent artery, U is the velocity at the centre of the parent artery and ν is the kinematic viscosity), the maximum axial velocity, shear strain rate and the recirculation length were measured for both eccentric and concentric models and compared with each other.

1. Introduction

Atherosclerotic plaques within coronary arteries result in coronary stenosis, compromising blood flow to the distal myocardium and resulting in local physiological perturbances such as recirculation and shear stress [1]. Coronary lesion severity is often graded by the amount of lumen encroachment or stenosis it causes, and most clinical decisions are based on lesion stenosis severity [2]. However, other lesion characteristics such as eccentricity [3,4] are determinants of both shear rate and the extent of flow recirculation in in-vitro and in computational fluid dynamics (CFD) analysis of the arteries [5]. It has been shown that 81% of the coronary lesions studied by intravascular sonography were eccentric, and eccentric lesions are more likely to occur in patients with cardiovascular symptoms [6-8]. Many studies have been performed numerically and experimentally to clarify the importance of stenosis asymmetry in different arteries. Young and Tsai [9] studied experimentally the flow through a stenosis using in-vitro models with symmetric and asymmetric stenosis. They noted that flow characteristics such as recirculation zone length and pressure losses are strongly dependent on the shape of the stenosis, such that models with asymmetric stenosis have a higher pressure drop and a

longer recirculation zone. Einav et al. [10] investigated platelet activation and aggregation level in eccentric and concentric stenosis models by CFD simulation and digital particle image velocimetry (DPIV). They demonstrated that the recirculation zone provides an optimal environment for procoagulant factor mixing and promoting activation of the coagulation system. They also indicated that eccentric stenosis induced more platelet aggregation than did the concentric stenosis model. Tambasco et al. [11] simulated carotid bifurcation models with eccentric and concentric stenosis. They found that eccentric stenosis is more prone to platelet activation and aggregation due to attenuated platelet deposition and plaque growth. They also concluded that eccentric stenosis may have a high potential for thrombus formation. Steinman et al. [12] investigated the effect of lesion geometry on post-stenotic recirculating flow and wall shear stress using CFD and digital particle image (DPI) methods. They identified that recirculation zone length and location and also wall shear stress are key parameters that differ between eccentric and concentric stenosis models. In our previous study [13], the effect of the lesion eccentricity on the flow behaviour was investigated numerically in a group of diseased human coronary arteries. It was shown that the effect of the stenosis severity is important than the lesion eccentricity effect on the blood flow behaviour; however, in a group of a patients with same stenosis severity, the lesion eccentricity could affect the flow recirculation and shear rate to a great extent.

In this study, a particle image velocimetry (PIV) method was implemented to analyse the effect of lesion eccentricity on the transient flow behaviour in coronary artery models and also to investigate the correlation between the Reynolds number (Re) and the eccentricity effect on flow behaviour.

2. Methods

2.1. Experimental technique

2.1.1. Stenosis artery models

Two eccentric and concentric stenosis models were manufactured from silicone (R'Tech Co. Ltd, Japan) (Fig. 1). All models were box-type with an inner diameter of 4 mm. The model sizes were based on the values of the human left main artery (LMA) and left anterior descending (LAD) [14]. The resultant models had a 70% diameter stenosis (DS) as defined by NASCET and calculated by equation (1).

$$DS = 1 - \frac{D_s}{D} \quad (1)$$

where D_s is the diameter of the stenosis and D is the diameter of the parent artery. The refractive index of the silicone models was 1.41, measured by using a refractometer (ATAGO, R5000, Japan).

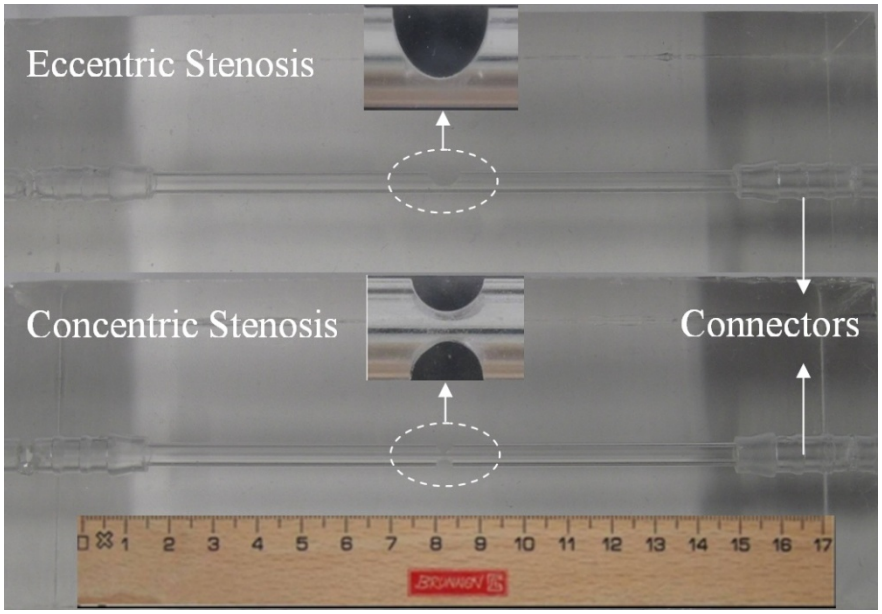

Fig 1. The silicone stenosis models

2.1.2. Flow circuit

The silicone stenosis models were connected to a particle image velocimetry (PIV) circuit as illustrated in Fig. 2. To achieve a fully-developed flow at the inlet of the models, 1.5 m of rigid pipe with the same internal diameter as the

silicone models was directly connected to the entrance of the models. An Nd:YAG solid laser (BWN-532-100E, B&W TEK Inc., USA) of wavelength 532 nm was used to produce a light sheet in the desired area of visualisation. The desired thickness and width of the light sheet were achieved by aligning a micro lens with 105 mm focal length and 2.8 F ratio (Micro-Nikkor, Nikon Co. Ltd., Japan).

The pulsatile flow waveform depicted in Fig. 3 was generated using a screw pump (NBL30PU, R'Tech Co. Ltd., Japan). To minimise the distortion of the laser beam and camera images, the refractive index of the working fluid should match the refractive index of the silicone models. To achieve this, a solution of glycerol aqueous (75 wt%) and NaI aqueous (25 wt%) with a viscosity of 4.665 mPas and density of 1.194 g/ml was chosen as the working fluid, the flow properties of which are comparable with previously reported blood properties [15]. The fluid was seeded with 17.41 micron cross-linked polystyrene particles with density of 1.2 g/ml. The settling velocity [16] was calculated to ensure that the difference between the density of the working fluid and the seeding particles was small enough to avoid falling or rising of the particles. A high-speed digital camera (Fastcam SA3, Photron Limited Co. Ltd., Japan) with a maximum of 10,000 frames per second (fps) was used to capture the motion of the particles and a total of 100 images were analysed for each PIV run.

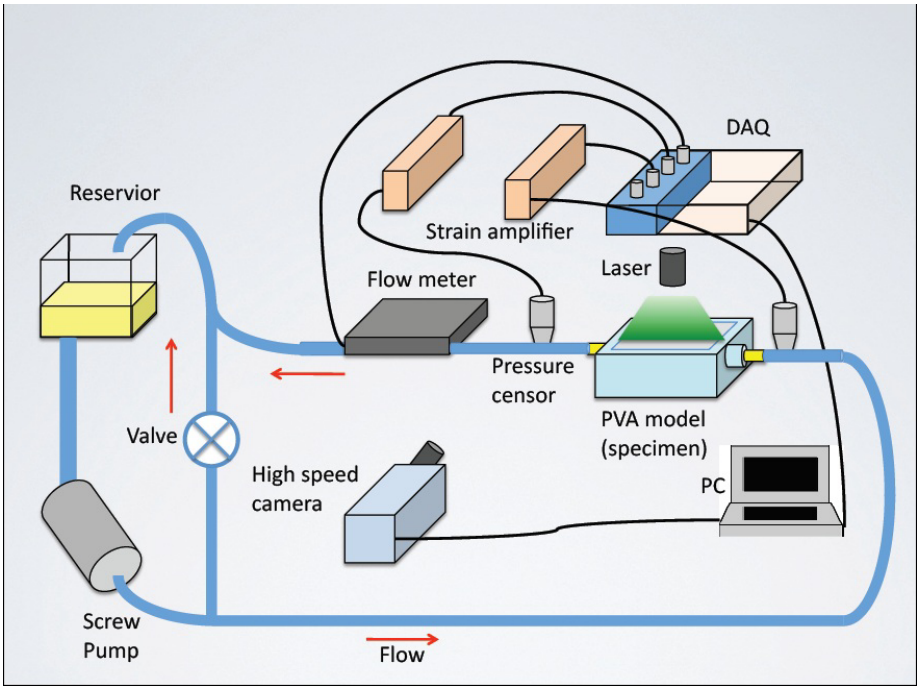

Fig 2. Diagram of PIV circuit

2.1.3. PIV measurement

The volumetric flow rate shown in Fig. 3 was measured and monitored by a Coriolis flowmeter (FD-SS2, Keyence Co. Ltd., Japan). In the PIV experiment, the displacements of the seeding particles were used to calculate the velocity gradient, shear strain rate and also to identify the recirculation zone. The geometry and the flow rate changes can result in great variations in the displacement of individual particles in regions of high velocity gradient. Therefore, using the same camera settings including frame per second (fps) rate, shutter speed and resolution at different locations and flow rates may fail to capture all fast and slow moving particles inside the interrogation area. To resolve this problem, as seen in Fig. 4, the data was collected at three different locations: 0-3 diameters upstream of the stenosis (Region (I)), at the stenosis (Region (II)), and 0-7 diameters downstream of the stenosis (Region (III)). At each location, several combinations of fps, shutter speed and resolution were tested to find the best camera settings.

The Reynolds number (Re) was calculated using equation (2), from the diameter of the parent artery (D).

$$\mathrm{Re} = \frac{\mathrm{DU_s}}{\upsilon} \qquad (2)$$

where υ is the kinematic viscosity and Us is the velocity at the centre of the parent artery.

The recordings were analysed using Davis software (Davis 7.2, La Vision Inc., Germany) with interrogation areas of 32×32 pixels and overlapped by 50%. The results for each time phase t were calculated as the average of the corresponding recorded images in the time interval of $t \pm \Delta t$ with $\Delta t = 0.005$ s.

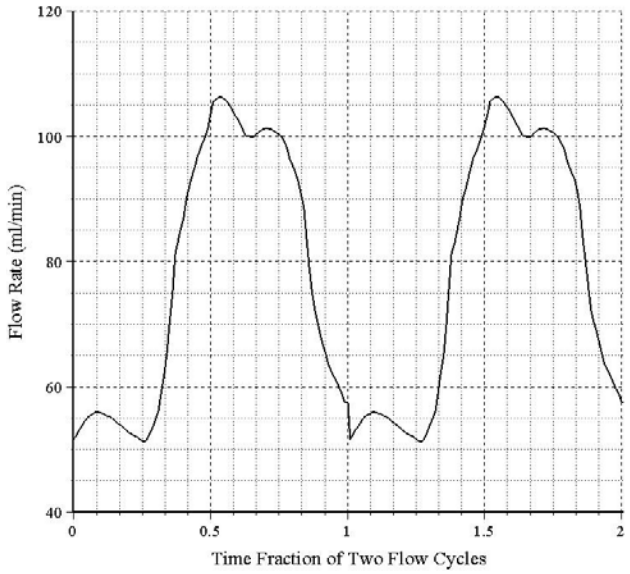

Fig 3. Flow waveform in the PIV experiment.

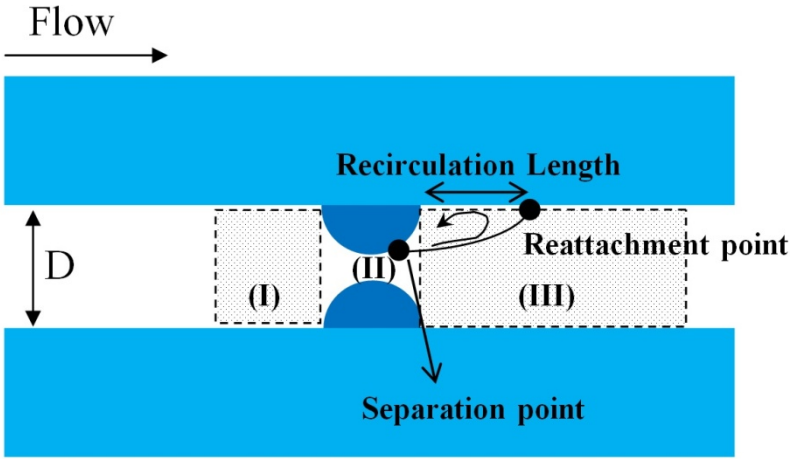

Fig 4. Flow and geometry of the artery model with a stenotic region.

2.2. Computational fluid dynamics

Computational fluid dynamics (CFD) analysis was performed using a slightly modified method from one that we have previously published [13]. In brief, the unsteady simulations were conducted using ANSYS CFX (ANSYS-Fluent Inc., Lebanon, NH, USA), employing a hexahedric grid with a nodal distance between 0.01 and 0.02 mm. A boundary layer mesh consisting of 4 rows with a growth factor of 1.2 was generated in accordance with current standards [17,18]. The flow for the simulation was assumed to be 3D, laminar and transient. The walls were considered solid and a stationary no-slip boundary condition was adopted at the walls. The flowing fluid was modelled as an incompressible Newtonian fluid with the same properties as the PIV working fluid. The flow rate waveform at the inlet and pressure waveform at the outlet recorded during the PIV experiment were set as the inlet and outlet boundary conditions, respectively. To achieve a periodic solution, the model was initially configured with the flow data from steady state simulation and then the model was run with a constant time step of 0.001 s over at least three cycles to satisfy the condition of the periodic solution.

3. Results

3.1. Comparison of PIV results for eccentric and concentric models

In Fig. 5(a) and (b), the impact of the eccentricity on the velocity contours is investigated at the time corresponding to Re = 85. As depicted, the eccentric model results in a higher velocity with stronger jetting behaviour passing the stenosis than in the concentric model. The streamline patterns downstream of the stenosis (Region (III), see Fig. 4) in both models are presented in Fig. 5(c) and (d). As shown, in the post-stenotic region, the eccentric stenosis causes the formation of a larger recirculation zone located on one side of the vessel, in contrast to the concentric stenosis, which produces a toroidal recirculation zone located along the circumference of the wall.

Fig. 6 compares (a) maximum axial velocity, (b) shear strain rate and (c) recirculation zone length of the eccentric and concentric models. The results are obtained during the flow cycle at nine different times corresponding to nine different Reynolds numbers. As expected, for both eccentric and concentric models, an increase in the Reynolds number results in an increase in the maximum axial velocity, shear strain rate and recirculation zone length. At all Re numbers, the eccentric model is associated with greater velocity, shear strain rate and recirculation zone length. Direct comparison of the eccentric and concentric models results reveals that the highest and lowest impact of the eccentricity are on the recirculation zone length and maximum shear strain rate, respectively.

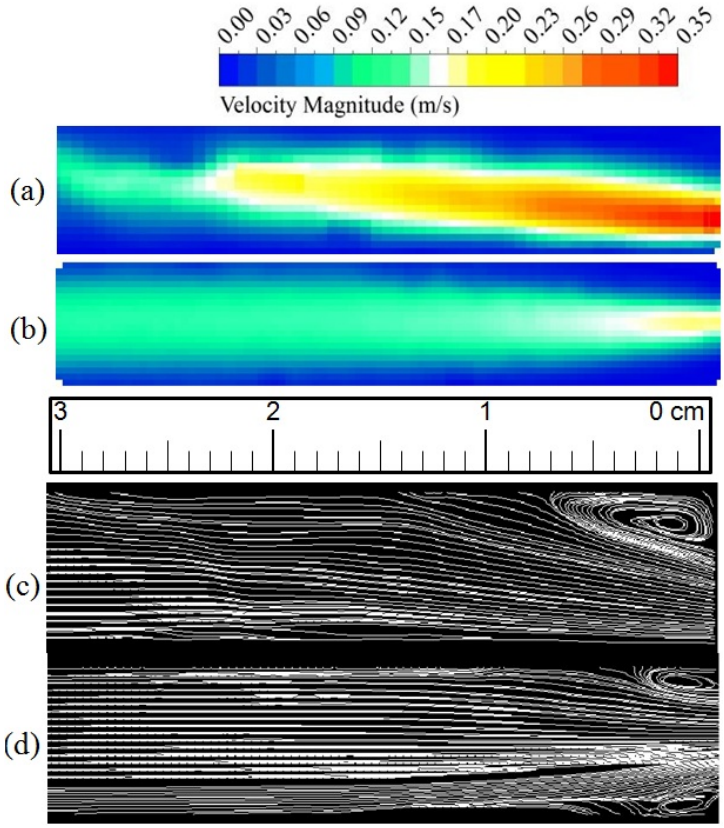

Fig. 5. (a) PIV velocity contours for eccentric model, (b) PIV velocity contours for concentric model, (c) PIV streamlines for eccentric model, and (d) PIV streamlines for concentric model.

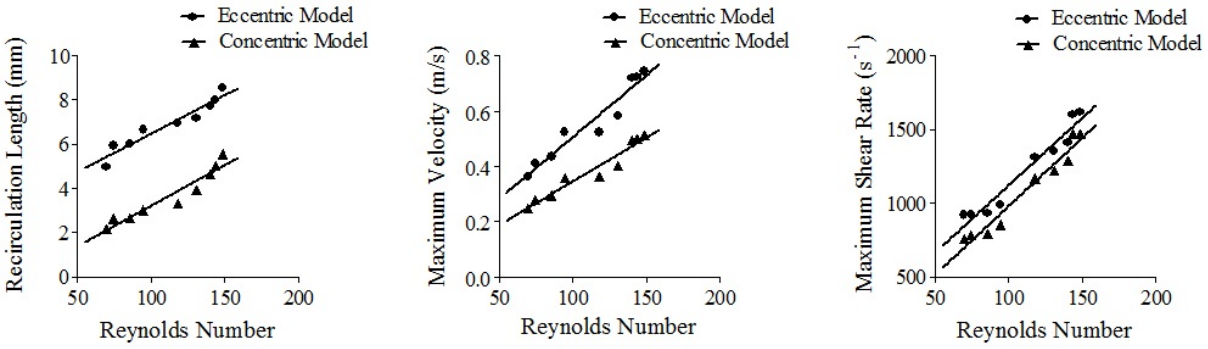

Fig. 6. Eccentric and concentric models comparison at different Re numbers (a) maximum velocity, (b) maximum shear strain rate, and (c) recirculation length.

To clarify the effect of the eccentricity, the parameters Φ_{DV}, Φ_{DS} and Φ_{DR} are defined showing the difference percentage of the maximum axial velocity, shear strain rate and recirculation zone length between eccentric and concentric models, respectively (Eqs. 3-5).

$$\Phi_{DV} = \frac{\mathrm{MaxVel}_{\mathrm{Eccentric}} - \mathrm{MaxVel}_{\mathrm{Concentric}}}{\mathrm{MaxVel}_{\mathrm{Eccentric}}} \times 100 \quad (3)$$

$$\Phi_{DS} = \frac{\mathrm{MaxShear}_{\mathrm{Eccentric}} - \mathrm{MaxShear}_{\mathrm{Concentric}}}{\mathrm{MaxShear}_{\mathrm{Eccentric}}} \times 100 \quad (4)$$

$$\Phi_{DR} = \frac{\mathrm{Recirculation}_{\mathrm{Eccentric}} - \mathrm{Recirculation}_{\mathrm{Concentric}}}{\mathrm{Recirculation}_{\mathrm{Eccentric}}} \times 100 \quad (5)$$

In Table 1, the values of the above parameters at different Reynolds numbers are summarised. As seen in Table 1, Φ_{DV}, Φ_{DS} and Φ_{DR} vary from 30.95 to 32.33, 8.47 to 17.22 and 35.08 to 56.21, respectively. The following conclusions can be drawn through analysis of these values:

- The highest and lowest impacts of eccentricity are on the recirculation zone length and the maximum shear strain rate, respectively.
- During the flow cycle, the Φ_{DV} varies by only %1.38; however, the Φ_{DS} varies by %21.13. Thus the transient nature of the flow has a negligible effect on the difference between the maximum axial velocities of the eccentric and concentric models; however, the difference between the recirculation zone lengths of the eccentric and concentric models is markedly affected by the transient nature of the flow.

Table 1
Difference percentage parameters at different Re numbers

Re	70	75	85	95	120	130	140	145	150
Φ_{DV}	32.24	32.29	32.33	31.69	31.03	30.95	31.17	31.04	31.02
Φ_{DS}	15.16	14.77	17.22	9.06	13.73	8.47	8.76	10.96	10.02
Φ_{DR}	49	54.97	56.21	54.79	52.53	45.54	39.71	36.98	35.08

In Fig. 7, the above defined parameters Φ_{DV}, Φ_{DS}, Φ_{DR} are presented as a function of Re number varying from 70 to 150. As depicted, as the Re number increasesΦ_{DV}, Φ_{DS}, Φ_{DR} decreases, indicating a negative correlation between Re number and Φ_{DV}, Φ_{DS}, Φ_{DR}. This means that at higher Re number, the difference between eccentric and concentric stenoses decreases and both eccentric and concentric stenoses tend to have same effect on the blood flow behaviour.

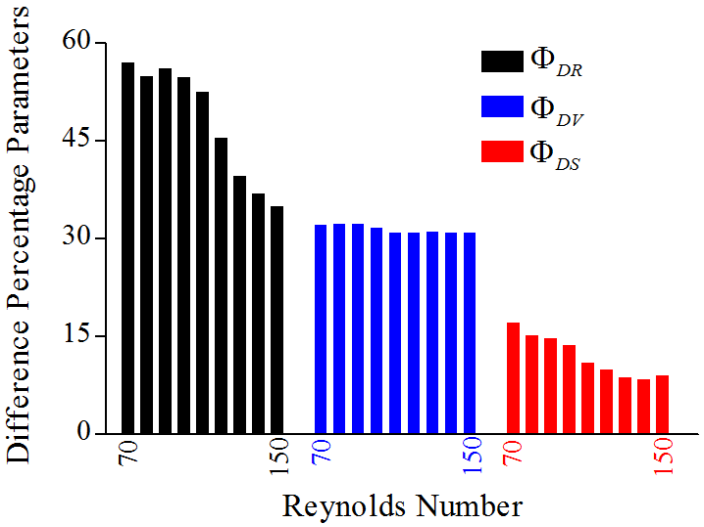

Fig. 7. Correlation between difference percentage parameters and Re number (a) Φ_{DV}, (b) Φ_{Ds}, and (c) Φ_{DR}.

3.2. CFD and PIV results comparison

At the time corresponding to Re = 85, the PIV and CFD velocity contours downstream of the stenosis in the eccentric model are compared in Fig. 8(a) and (b). As shown, there is a good agreement between the PIV and CFD predicted velocity contours, with slightly higher predictions for the PIV values. In Fig. 8(c) and (d), at t = 0.2 s, the recirculating flow regions captured by the PIV and CFD methods are shown for the eccentric model. Deceleration and reversal of flow are observed downstream of the stenosis, with the presence of a recirculation zone leading to greater residence times. Both methods predict a recirculating flow of roughly the same length; however, the recirculating flow height predicted from the CFD simulation is slightly greater than that from the PIV. The CFD and PIV computed maximum axial velocities and shear strain rates for the eccentric model are compared throughout the flow cycle in Fig. 9(a) and (b). As seen, the PIV predicted maximum velocity and maximum shear strain rate agree well with the CFD results and the behaviour is reasonably similar throughout the flow cycle. However, better agreement is evident for the maximum velocity than the shear strain rate. The correlation values of CFD and PIV computed maximum velocity and shear strain rate are 0.91 and 0.75 respectively.

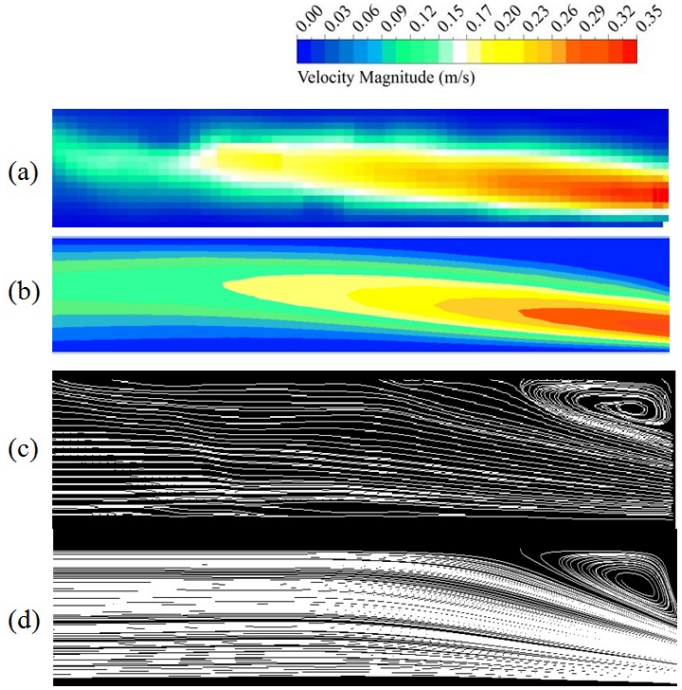

Fig. 8. Eccentric model downstream at time corresponding to Re = 85 (a) PIV velocity contours, (b) CFD velocity contours, (c) PIV streamlines, and (d) CFD streamlines.

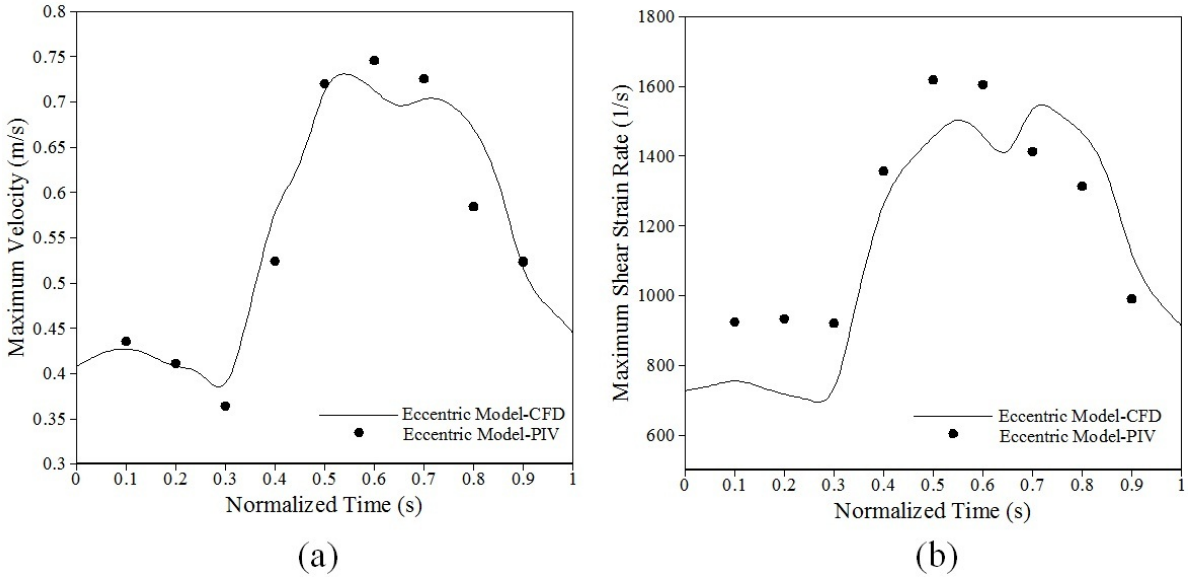

Fig. 9. Comparison between the PIV and CFD throughout the flow cycle (a) maximum velocity and (b) maximum shear strain rate.

4. Discussion and conclusions

In this study, a transient PIV experiment was conducted with two coronary artery models with eccentric and concentric stenosis configurations to examine the effect of the eccentricity on the length of the recirculation zone, the maximum shear strain rate and the maximum velocity at different times of the flow cycle corresponding to different Reynolds numbers.

4.1. Stenosis eccentricity effects

The PIV results showed that during the flow cycle, the eccentric model was always associated with greater recirculation zone length, maximum shear strain rate and maximum axial velocity than the values for the concentric lesion, a finding that is in a good agreement with previous studies [5, 13]. The analysis of the results revealed that at high Reynolds numbers the difference between the eccentric and concentric models decreased. This can be examined by comparing the velocity profiles downstream of the stenosis for the eccentric and concentric models at low and high Reynolds numbers (Fig. 10). As seen, at higher Reynolds numbers, the gradient between the velocity profiles of the eccentric and concentric models (α_2) is less than that of the low Reynolds numbers (α_1). This means that the similarity between the velocity profiles of the eccentric and concentric models increases as the Reynolds number increases. The shear strain rate depends on the velocity profile and the recirculation length is also dependent on the shear strain of the flow. Therefore, the velocity profile analysis verified that the difference between the flow behaviour of the eccentric and concentric models decreases as the Reynolds number increases.

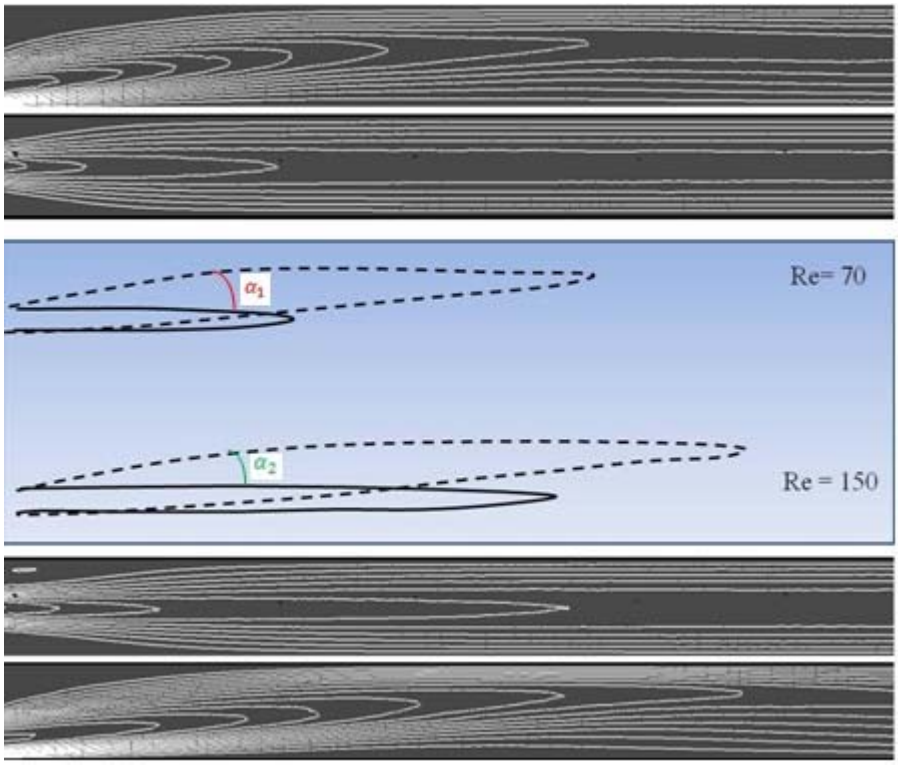

Fig. 10. Velocity profiles downstream of the stenosis for the eccentric and concentric models at low and high Re numbers.

4.2. CFD validation

A transient CFD simulation was performed and compared with the PIV measurements conducted in the eccentric coronary artery model. Good agreement was found between the PIV and CFD predicted maximum axial velocities, maximum shear strain rates and recirculation zone lengths. However, the greatest and least discrepancies between the results were observed for maximum shear strain rate and maximum axial velocity, respectively. The quantitative difference between the maximum shear strain rates was attributed to the inability of the PIV method to capture near-wall velocities; however, the qualitative behaviour of the PIV predicted maximum shear strain rate was reasonably similar to that of the CFD result.

5. Limitations

The main limitation of this study relates to the geometrical properties of the experimental models. The coronary arteries have complex vessel characteristics such as curvature and branching. Our PIV model assumes laminar flow with Newtonian fluid properties and non-deformable vessel wall. However, previous studies have shown that these assumptions are acceptable for simulations involving human arteries [19, 20]. Other vessel characteristics such as curvature, bifurcations and vessel size will also likely affect the flow parameters measured. This study attempted to control for these confounding effects by using simple models of eccentric and concentric arteries. Because the study was restricted to only simple artery models, the absolute values derived cannot be generalized to the human arteries. However, we believe that the general concepts will still be applicable to the all human arteries. In addition, the PIV facility used in this study was not capable of capturing near-wall velocities which might affect the shear strain results. The natural coronary flow profile in the coronary arteries is different from the flow rate produced by the PIV pump.

Acknowledgments

The authors wish to acknowledge Tohoku University's Global COE Program and World Centre of Education and Research for assistance in performing the studies.

Conflict of interest

None.

References

[1] Asakura T, Karino T. Flow patterns and spatial distribution of atherosclerotic lesions in human coronary arteries. Circ Res. 1990; 66: 1045-66.

[2] Shaw LJ, Berman DS, Maron DJ, Mancini GB, Hayes SW, Hartigan PM, Weintraub WS, O'Rourke RA, Dada M, Spertus JA, Chaitman BR, Friedman J, Slomka P, Heller GV, Germano G, Gosselin G, Berger P, Kostuk WJ, Schwartz RG, Knudtson M, Veledar E, Bates ER, McCallister B, Teo KK, Boden WE. Optimal medical therapy with or without percutaneous coronary intervention to reduce ischemic burden: results from the Clinical Outcomes Utilizing Revascularization and Aggressive Drug Evaluation (COURAGE) trial nuclear substudy. Circulation 2008; 117: 1283-91.

[3] Li F, McDermott MM, Li D, Carroll TJ, Hippe DS, Kramer CM, Fan Z, Zhao X, Hatsukami TS, Chu B, Wang J, Yuan C. The association of lesion eccentricity with plaque morphology and components in the superficial femoral artery: a high-spatial-resolution, multi-contrast weighted CMR study. J Cardiovasc Magn Reson 2010; 12: 37.

[4] Yamagishi M, Terashima M, Awano K, Kijima M, Nakatani S, Daikoku S, Ito K, Yasumura Y, Miyatake K. Morphology of vulnerable coronary plaque: insights from follow-up of patients examined by intravascular ultrasound before an acute coronary syndrome. J Am Coll Cardiol. 2000; 35(1): 106-111.

[5] Poepping TL, Rankin RN, Holdsworth DW. Flow patterns in carotid bifurcation models using pulsed Doppler ultrasound: effect of concentric vs. eccentric stenosis on turbulence and recirculation. Ultrasound Med Biol. 2010; 36(7): 1125-1134.

[6] Yamagishi M, Terashima M, Awano K, et al. Morphology of vulnerable coronary plaque, Insights from follow-up of patients examined by intravascular ultrasound before an acute coronary syndrome. J Am Coll Cardiol. 2000; 35: 106-11.

[7] Ojio S, Takatsu H, Tanaka T, et al. Considerable time from the onset of plaque rupture and/or thrombi until the onset of acute myocardial infarction in humans. Coronary angiographic findings within 1 week before the onset of infarction. Circulation 2000; 102: 2063-69.

[8] Ohara T, Toyoda K, Otsubo R, Nagatsuka K, Kubota Y, Yasaka M, Naritomi H, Minematsu K. Eccentric stenosis of the carotid artery associated with ipsilateral cerebrovascular events. AJNR Am J Neuroradiol. 2008; 29: 1200-1203.

[9] Young DF, Tsai FY, Flow characteristics in models of arterial stenoses-I. Steady flow. J Biomechanics 1973; 6: 395-410.

[10] Einav S, Bluestein AD. Dynamics of blood flow and platelet transport in pathological vessels. Ann N.Y. Acad Sci. 2004; 1015: 351-366.

[11] Tambasco M, Steinman DA. Path-dependent hemodynamics of the stenosed carotid bifurcation. Ann Biomed Eng. 2003; 31: 1054-65.

[12] Steinman DA, Poepping TL, Tambasco M, Rankin RN, Holdsworth DW. Flow Patterns at the Stenosed Carotid Bifurcation: Effect of Concentric versus Eccentric Stenosis. Ann Biomed Eng. 2000; 28: 415-423.

[13] Javadzadegan A, Yong ASC, Chang M, Ng ACC, Yiannikas J, Ng MKC, Behnia M, Kritharides L. Flow recirculation zone length and shear rate are differentially affected by
stenosis severity in human coronary arteries. AJP-Heart Circ Physiol. 2013; 304: 559-566.

[14] Dodge JT, Brown BG, Bolson EL, Dodge HT. Lumen diameter of normal human coronary arteries. Influence of age, sex, anatomic variation, and left ventricular hypertrophy or dilation. Circulation 1992; 86: 232-246.

[15] Patel D .J, Vaishnavr N. Basic hemodynamics and its role in disease processes. Baltimore: University Park Press; 1980.

[16] Blake JR, Easson WJ, Hoskins PR. A dual-phantom system for validation of velocity measurements in stenosis models under steady flow. Ultrasound in Med. & Biol. 2009; 35: 1510-1524.

[17] Myers JG, Moore JA, Ojha M, Johnston KW, Ethier CR. Factors influencing blood flow patterns in the human right coronary artery. Ann Biomed Eng. 2001; 29: 109-120.

[18] Prakash S, Ethier CR. Requirements for mesh resolution in 3-D computational hemodynamics. J Biomed Eng. 2001; 123: 26-38.

[19] Feldman CL, Ilegbusi OJ, Hu Z, Nesto R, Waxman S, Stone PH. Determination of in vivo velocity and endothelial shear stress patterns with phasic flow in human coronary arteries: a methodology to predict progression of coronary atherosclerosis. Am Heart J. 2002;143(6):931-939.

[20]Torii R, Keegan J, Wood NB, Dowsey AW, Hughes AD, Yang GZ, Firmin DN, McG Thom SA, Xu XY. The effect of dynamic vessel motion on haemodynamic parameters in the right coronary artery: a combined MR and

CFD study. Br J Radiol. 2009; 82 Spec No 1:S24-32.